Effect of Ionic Strength on Bubble Coalescence in Inorganic Salt and Seawater Solutions

Joshua M. Sovechles and Kristian E. Waters
Dept. of Mining and Materials Engineering, McGill University, Montreal, QC, Canada H3A 0C5

DOI 10.1002/aic.14851
Published online May 12, 2015 in Wiley Online Library (wileyonlinelibrary.com)

Bubble size is of fundamental importance in the flotation process, as it provides the surface area for particle collection. Typically, weak surfactants (frothers) are added to process water to reduce bubble coalescence. Certain inorganic electrolytes, which occur naturally in some flotation process water, have been shown to mimic the role of frothers. The concentration at which bubble coalescence is inhibited, the critical coalescence concentration, was determined in a 5.5-L mechanical flotation cell for a series of coalescence inhibiting inorganic salts. To mimic some industrial flotation process water, a synthetic sea salt solution was also tested. It was found that when the multicomponent sea salt solution was broken down into its constituent parts, the addition of the ionic strength of each ion correlated well with the overall ionic strength curve of all the salts tested. The critical coalescence ionic strength ranged from 0.22 to 0.35, with sea salt being 0.26. © 2015 American Institute of Chemical Engineers *AIChE J*, 61: 2489–2496, 2015
Keywords: bubble size, bubble coalescence, critical coalescence concentration, critical coalescence ionic strength, inorganic salt, seawater, flotation

Introduction

Froth flotation facilitates the separation of valuable materials from low grade ore bodies through differences in hydrophobicity and bubble-particle interactions. Bubble size, which is controlled by a combination of bubble coalescence and break-up phenomena, plays an important role in flotation kinetics as it is a surface area driven process. The flotation process typically takes place within a mechanically agitated cell. The turbulent mixing zone around the impeller-stator assembly acts to maintain the slurry suspension and to break the introduced air into small bubbles. Bubble-particle agglomerates rise through the progressively laminar flow as they approach the top of the cell to be collected in the froth phase. Air is either drawn in from the vacuum created by the impeller or is forced in with the use of an external blower Typically organic chemicals, known as frothers, are employed in flotation circuits to facilitate air dispersion into fine bubbles and to stabilize froth formation. Cho and Laskowski[1] introduced the concept of a critical coalescence concentration (CCC), which is defined as the frother concentration at which bubble coalescence inhibition is at a maximum. The CCC is now an accepted parameter in the characterization of frothers. The Sauter mean diameter (D_{32}) is calculated from the measured bubble size distribution (BSD) and then plotted as a function of frother concentration (C). The D_{32}-C curve, shown in Figure 1, is characterized by a sharp initial decrease in D_{32} which then reaches a plateau. The slope of the curve in Zone I is dependent upon the solutes ability to prevent coalescence, while the value of the limiting bubble size, d_l, is considered a property of the bubble break-up mechanics.[2] The point at which the fitted curves for Zones I and II meet defines the CCC.

Recently, froth flotation and gas dispersion in saline solutions have generated much attention. Certain inorganic electrolytes have been shown to mimic the role of frothers by inhibiting bubble coalescence leading to a decreased bubble size in the pulp phase.[1,3–10] Salts are not intentionally added to achieve bubble size reduction due to the high concentrations (0.02–0.8 M) required,[7,11] when compared to frothers (5–20 ppm). However, in an effort to minimize fresh water use, many industrial flotation circuits have introduced the use of underground water or seawater as conventional practice, thus inorganic salts may be present naturally.[6] In a number of applications, (e.g., flotation of base metal sulfides in brines or seawater) frothers are still used in concentrated electrolyte solutions.[12] One such case, the Raglan mine and mill in northern Canada, has managed to successfully run its flotation circuits without the use of frothers for many years.[6]

Bubble coalescence is a particularly complex phenomenon especially when it takes place in saline water or seawater, as both surface active compounds (frothers) and surface-inactive compounds (inorganic salts) are able to stabilize bubbles against coalescence and thus reduce bubble size. Several researchers have attempted to quantify the effect of inorganic salts on bubble coalescence, with a common measure of the effect of inorganic salts on bubble coalescence being the transition concentration (TC). The TC of a salt is the point at which there is a sharp decrease in coalescence events, and is used when coalescence events and not bubble size is measured. There has been much debate over the mechanisms behind the ability of salts to inhibit coalescence

Correspondence concerning this article should be addressed to K. E. Waters at kristian.waters@mcgill.ca.

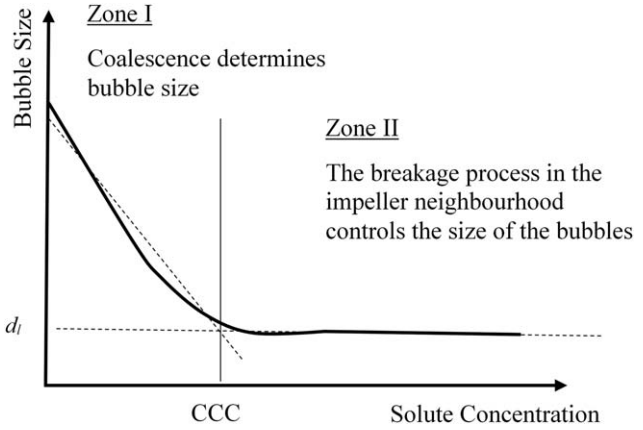

Figure 1. Schematic diagram of the effect of solute concentration on bubble size in a flotation cell (Adapted from Elsevier).

and, as yet, there is no definitive agreement. The Marangoni effect, surface rheology, colloidal forces, gas solubility, and ion specific effects are all included in the leading theories explaining the stabilizing effect of salts on bubble coalescence at salt concentrations above the TC. A comprehensive review of all theories is detailed by Firouzi et al.[13]

Lessard and Zieminski[5] and Christenson et al.[14] brought bubbles into contact using adjacent capillaries and evaluated the coalescence percentage as a function of solute concentration. They observed the existence of a TC at which coalescence was sharply reduced. The TC was defined as the concentration at which 50% of the contacted bubbles coalesced (TC_{50}). Craig et al.[7] determined the TC for a range of inorganic salts using a bubble swarm produced from air flowing through a glass sinter. A laser beam was passed through the swarm and a detector measured the transmission. TC was determined to be when transmission was 50% of the range from water only (assumed 100% coalescence) to the concentration giving minimum transmission (assumed complete coalescence inhibition).

Marrucci and Nicodemo[4] measured the average bubble size (via image analysis) produced by a porous plate, in the presence of a number of different electrolytes, in a laboratory-scale flotation column. For all salt types tested, an increase in concentration lead to a decrease in the average bubble diameter until a stable minimum was reached. This minimum value was independent of salt type, however, the concentration at which the minimum was reached was specific to each salt. Salts containing polyvalent ions tended to decrease bubble size at lower molar concentrations. The conclusion reached was that the electrolytes increased the electrical repulsive forces at the bubble surface, inhibiting coalescence between bubbles. Using this data Prince and Blanch[15] defined the TC as the concentration at which a minimum bubble size was reached, termed TC_{100} by Quinn et al.[9] (similar in nature to CCC).

All aforementioned studies have shown that the TC is lower for multivalent ions than for monovalent ions, for those salts that display a coalescence inhibiting behavior. Furthermore, correlations have been found between solution ionic strength and either bubble size or gas holdup.[6,16–18] Ionic strength cannot be taken as a universal rule, however, as certain salts (e.g., $NaClO_4$, KI, and KNO_3) show extremely weak coalescence inhibition[4,14] and do not follow the ionic strength rule. In addition, Craig et al.[7] observed that certain electrolytes have no effect on bubble coalescence, even at very high concentrations (~0.5 M), and rules based on the nature of the cationic/anionic pair were established to predict this behavior.

More recently Castro et al.[19] and Quinn et al.[9] applied the CCC concept to inorganic salts as the same general shape of the D_{32}-C curve is observed. The aim of the present study was to expand on the work of Quinn et al.[9] by determining the CCC for a range of salts commonly encountered in flotation systems, and to investigate the concept of ionic strength dependence. A synthetic sea salt solution was also tested in an attempt to study the cumulative strength of different ions in combined mixtures, to represent industrial flotation circuits that contain multiple inorganic salts, or use seawater.

Table 1. Chemical Specifications and Concentrations Tested

Chemical	Manufacturer	Grade	Concentrations Tested
NaCl	Fisher Scientific	ACS	0–1.5 M
KCl	Fisher Scientific	ACS	0–1.5 M
Na_2SO_4	Fisher Scientific	ACS	0–1 M
$CaCl_2$	Sigma Aldrich	≥96%	0–1 M
$MgCl_2$	Sigma Aldrich	>95%	0–1 M
$MgSO_4$	Sigma Aldrich	>99.5%	0–1 M
$AlCl_3$	Sigma Aldrich	>98%	0–0.25 M
$Al_2(SO_4)_3$	Fisher Scientific	Technical	0–0.25 M
Sea salt	Instant Ocean	Commercial	0–200% Seawater

Experimental

Materials

The list of chemicals used in this research is detailed in Table 1. These salts were chosen as they include the major ions found in many industrial flotation circuits.[12] A total of three tests were performed for all salts, to ensure reliable data. Concentrations were chosen based on literature data in an attempt to straddle the CCC and TC values and clearly define the slope and plateau of the CCC curve. Table 2 gives some TC and CCC data used to determine the initial salt concentrations tested. Ten or eleven concentrations were tested for each solute.

Apparatus

Experiments were conducted using a Denver D-12 laboratory-scale mechanical flotation machine (Serial: TCS-1101-3,

Table 2. Transition Concentration and CCC for Inorganic Salts Tested

	Bubble Swarm		Capillary
Solute Type	CCC or TC_{100} (M)	TC_{50}* (M)	TC_{50}† (M)
KCl	0.21‡–0.31§	0.120	0.202–0.23
NaCl	0.31§–0.778¶	0.078	0.145–0.208
Na_2SO_4	0.13§	–	0.051–0.061
$CaCl_2$	0.11§	0.037	0.055–0.060
$MgCl_2$	–	–	0.055
$MgSO_4$	0.07§	0.020	0.032–0.036
$AlCl_3$	0.05‡	–	0.035
$Al_2(SO_4)_3$	–	–	–

*Ref 7
†Ref 5, 11 and 14
‡Ref 4
§Ref 9
¶Ref 19

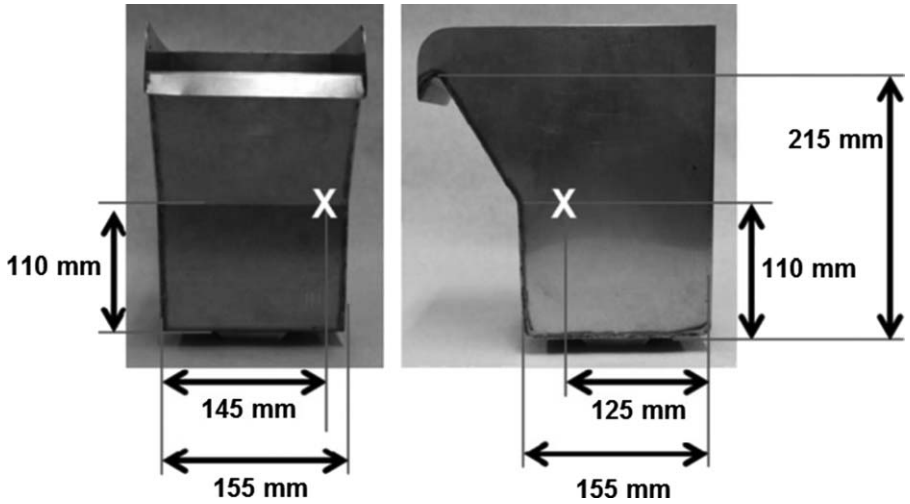

Figure 2. Dimensions of flotation cell (X indicates bubble sample location).

Size: D-1 FLOT) equipped with a 5.5-L (active volume) cell (Figure 2). The variable speed impeller was operated at 1600 rpm and the air flow rate was maintained at 0.11 dm^3/s (equivalent to a superficial gas velocity of 0.50 cm/s at point X, Figure 2) using an Omega flow meter (model FMA A2411). The entire experimental setup is shown in Figure 3. Two-phase (solution-air) tests were performed using deionized (DI) water which had been allowed sufficient time to reach room temperature (18–22°C). To maintain constant solution level throughout the experiment, the cell was filled to capacity and allowed to overflow as the test progressed. Bubbles were sampled at point X using the McGill Bubble Viewer. Bubbles rose through the vertical sampling tube (16 mm inner diameter and 900 mm in length) and into the viewing chamber (240 mm diameter by 140 mm depth) filled with test solution. An arrangement of light emitting diodes (Phlox, model LLUB-Q-1R-24V) covering an area of 100 mm × 100 mm were used to back-light the viewing chamber. Inside the chamber, bubbles contacted the inclined (15°) window and dispersed into a near monolayer.[20] Images of the bubbles sliding up the inclined window were taken using a Canon EOS 60D camera (equipped with a Canon EF 100 mm 1:1.28 USM macrolens) at a rate of 0.5–1 frames per second (depending on bubble rise velocity). These images were then analyzed offline to enable a large number of bubbles, recommended to be greater than 5000 by Hernandez-Aguilar et al.,[21] to be counted and give statistically robust results. A minimum of 10,000 bubbles were measured for each experiment. Image resolution was approximately 165 pixels/mm and picture size was approximately 35 mm (l) by 23 mm (h).

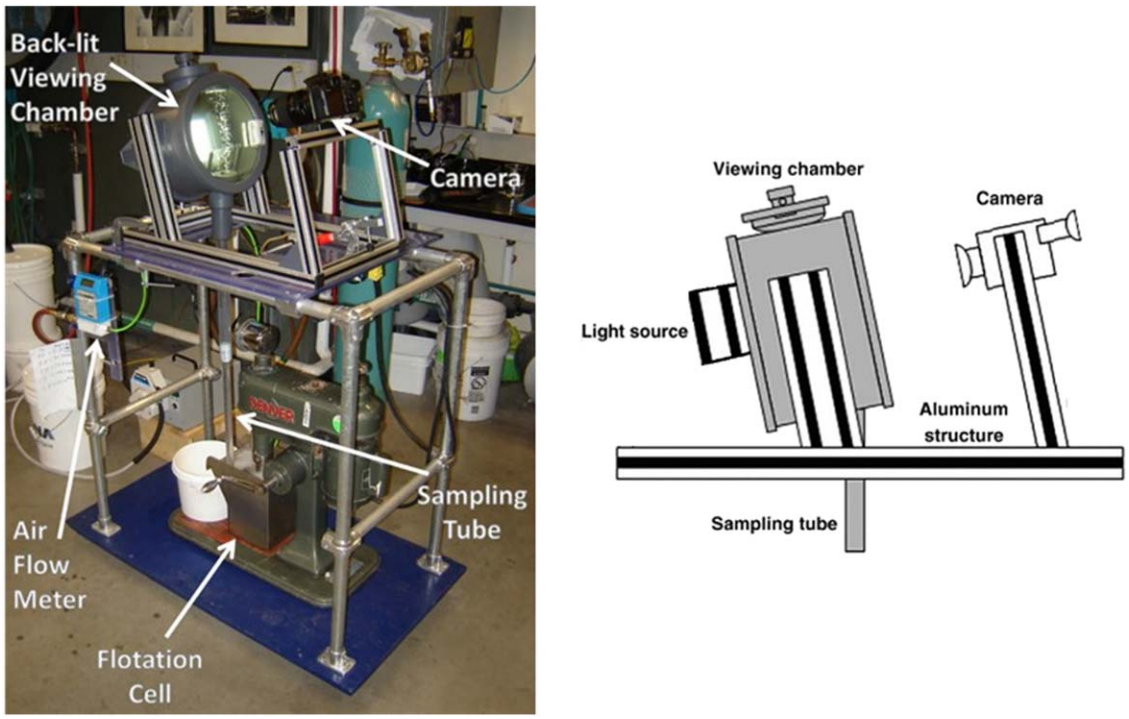

Figure 3. Bubble viewer in operation (left) and a schematic of the bubble viewer (right).

[Color figure can be viewed in the online issue, which is available at wileyonlinelibrary.com.]

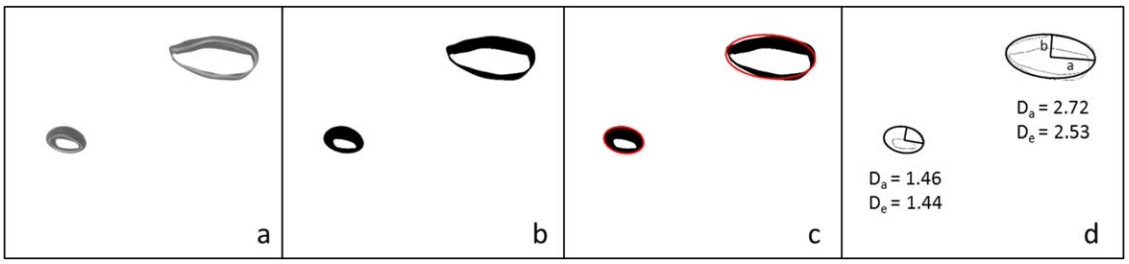

Figure 4. Image analysis procedure: (a) original bubble image, (b) image after applying threshold, (c) ellipse fitting, and (d) determination of major (a) and minor (b) semiaxes.

The bubble diameters calculated using both techniques are also shown. [Color figure can be viewed in the online issue, which is available at wileyonlinelibrary.com.]

Image analysis bubble sizing

The BSD was determined offline via the use of macro inside of the ImageJ© software. Calibration was conducted using a transparent rule in the plane of focus, which can be used to determine the number of pixels per millimeter. To measure the size of each bubble, a simple threshold is applied to discriminate between bubbles and the illuminated background. The automated image analysis procedure then tabulate the projected bubble area, A_p (mm^2), which was used to determine the projected area diameter, D_a (mm)[22,23]

$$D_a = \sqrt{4A_p/\pi} \tag{1}$$

The Sauter mean bubble diameter, D_{32} (mm) was calculated from

$$D_{32} = \frac{\Sigma D_a^3}{\Sigma D_a^2} \tag{2}$$

Alternatively, following the method detailed by Quinn et al.,[24] the sphere-volume equivalent diameter, D_e (mm), was calculated using the major (a) and minor (b) semiaxes of an ellipse fitted to the projected bubble area. This process is shown in Figure 4. Assuming the bubble to be a prolate ellipsoid, D_e was calculated using Eq. 3

$$D_e = \sqrt[3]{(2a)^2 \times (2b)} \tag{3}$$

The results from this method were found to match the projected area diameter closely for small bubble sizes (<1 mm), as seen in Figure 4. Above this range, however, it tended to underestimate the bubble size due to the nature of fitting an ellipse to the irregular bubble shapes typically seen with larger bubbles. The assumption of a prolate ellipsoid also becomes less likely with larger major to minor axis ratios. Therefore the projected area method was used to maintain consistency through the data analysis.

Data fitting—CCC models

A typical curve for the effect of salt concentration on bubble size in a mechanical flotation cell is shown in Figure 1.[2] Grau et al.[2] used a graphical method to estimate the CCC by fitting a straight line to the data in Zones I and II separately and noting there intersect as the CCC. However, more recently Nesset et al.[25] suggested fitting the D_{32}-C data with the following three-parameter model

$$D_{32} = D_l + A\exp[-B * C] \tag{4}$$

where D_l (mm) is the limiting D_{32} as the salt concentration tends toward infinity; A (mm) is the difference between D_l (mm) and the D_{32} in water (no solute present); B is the decay constant, and C is the solute concentration (M). The model allows for calculation of CCC_X (Eq. 5), the concentration at which the D_{32} is reduced by $X\%$ from that in pure water to the D_l. Nesset et al.[25] suggested that CCC_{95} accurately represents a measure of the CCC for frothers, and has been shown to be applicable for salts[9,19]

$$CCC_X = -\frac{\ln(1-X)}{B} \tag{5}$$

A distinct advantage of this method is the automation when calculating the CCC value, however, it does have some deficiencies. The model overestimated the CCC point when compared to the traditional graphical method. The model is constricted to pass through the D_{32} measured in water. This limits CCC calculations to the accuracy of this one measured point. A suggested solution is to add an extra term E, shown in Eq. 6, to represent the error in measurement at zero solute concentration. The values for E and B can then be solved iteratively to minimize the sum of the squared errors between measured values and the model. As the multiple tests should originate from the same initial point, the E value calculated from each salt can be averaged and a new zero concentration bubble size can be produced

$$D_{32} = D_l + (A+E)\exp[-B * C] \tag{6}$$

This did improve the estimate of the CCC, however, following a statistical analysis on the fit the model gave to the data points (hence the predicted CCC point), a further alteration was proposed. It was found that when the exponential decay component varied as a function of salt concentration the estimated CCC values were closer to those predicted by the graphical technique and the error variance from the data was reduced. Equation 7 shows this alteration

$$D_{32} = D_l + (A+E)\exp[(-B * C) * C] \tag{7}$$

Gomez et al.[26] provided an alternate way to model the CCC curve without the need for a DI water test. It was modeled by adding two contributions. The first was characterizing the effect of surface tension, which was determined by fitting an exponential function to the results for high concentrations (Zone II). The other was characterizing coalescence control, which was obtained by fitting a second exponential function to the low concentrations results (Zone I) with surface tension effects subtracted. The equation to calculate bubble size as a function of salt concentration was obtained by summation of both contributions[26]

$$D = a_{st}e^{b_{st}C} + a_{cc}e^{b_{cc}C} \tag{8}$$

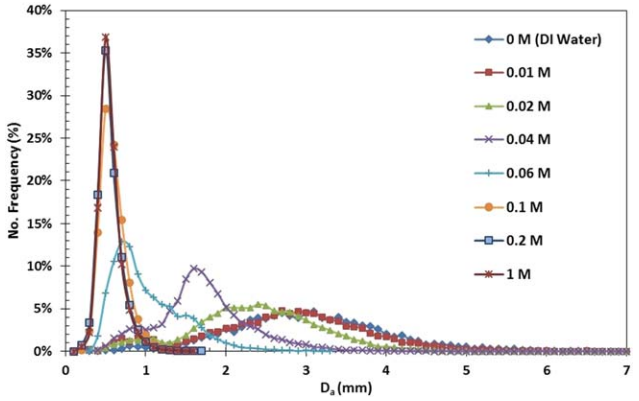

Figure 5. Bubbles size distributions in calcium chloride solutions.

[Color figure can be viewed in the online issue, which is available at wileyonlinelibrary.com.]

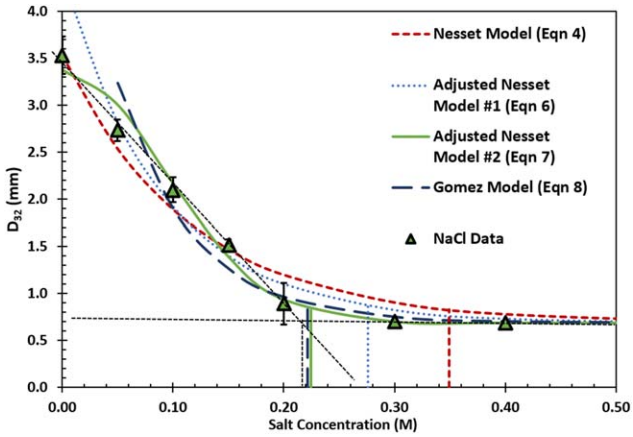

Figure 7. The Sauter mean diameter (D_{32}) as a function of salt concentration for sodium chloride, with the four aforementioned models and graphical technique shown.

[Color figure can be viewed in the online issue, which is available at wileyonlinelibrary.com.]

where D (mm) is bubble size; C (M) is the concentration of the salt solution; a and b are fitting parameters for the surface tension (subscript st) and coalescence control (subscript cc) contributions. The CCC value was calculated, using Eq. 9, as the concentration at which coalescence increased bubble size by 0.20 mm over the value predicted considering only surface tension effects. This value was selected as it was equal to the average error (95% confidence interval) associated with the bubble size measurements in the region of transition between Zones I and II; and is therefore the first measurable point of difference

$$\mathrm{CCC} = -\frac{\ln\left(\mathrm{error}_{\mathrm{meas}}/a_{\mathrm{cc}}\right)}{b_{\mathrm{cc}}} \tag{9}$$

Results

Figure 5 shows the progression of the BSD of calcium chloride, with examples of the corresponding bubble images appearing in Figure 6. As the concentration was increased, the BSD shifted from a wide distribution to a narrow distribution at a finer bubble size. At concentrations 0.1 M and above (which corresponds to the CCC_{95} of 0.09 M for $CaCl_2$), the distributions appear to be almost identically centered at approximately 0.6 mm.

Figure 7 shows the data for sodium chloride, along with the curves and CCC values from the four described models and the graphical method. It can be seen that the adjusted Nesset model, the Gomez model, and the traditional graphical method all produce similar results (~0.22 M). For the rest of the figures, the model shown is the adjusted Nesset model #2 (Eq. 7). Although similar results were obtained with the model by Gomez et al.,[26] the Nesset model is more established in industry and was, therefore, chosen as the basis for CCC calculation.

Figures 8–10 show the Sauter mean bubble diameter as a function of concentration for all of the tested salts, with the respective CCC_{95} values and confidence intervals displayed in Table 3. The CCC_{95} decreased for salts containing multivalent ions: The two 1:1 (cation:anion charge) salts KCl (0.25 M) and NaCl (0.22 M) had the highest CCC_{95}; the 1:2 and 2:1 salts Na_2SO_4 (0.08 M), $CaCl_2$ (0.09 M), and $MgCl_2$ (0.09 M) had intermediate CCC_{95} values; while the 2:2, 3:1, and 3:2 salts, $MgSO_4$ (0.07 M), $AlCl_3$ (0.06 M), and $Al_2(SO_4)_3$ (0.02 M), respectively, had the smallest CCC_{95} that decreased in value with increasing ionic strength.

The data in Figures 8–10 were replotted as a function of ionic strength (Figure 11). The data appear to follow a single

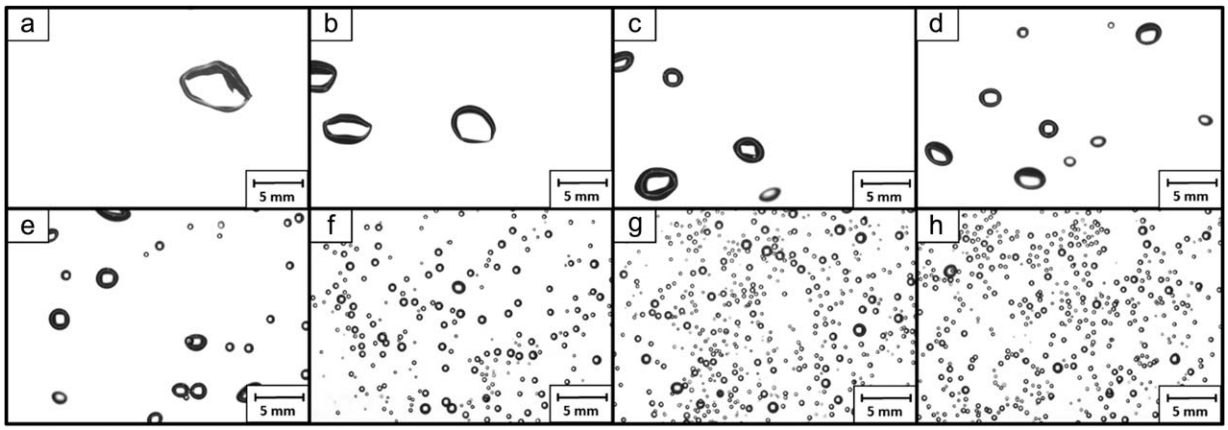

Figure 6. Example bubble size images in (a) distilled water, (b) 0.01 M $CaCl_2$, (c) 0.02 M $CaCl_2$, (d) 0.04 M $CaCl_2$, (e) 0.06 M $CaCl_2$, and (f) 0.10 M $CaCl_2$, (g) 0.20 M $CaCl_2$, and (h) 1.0 M $CaCl_2$.

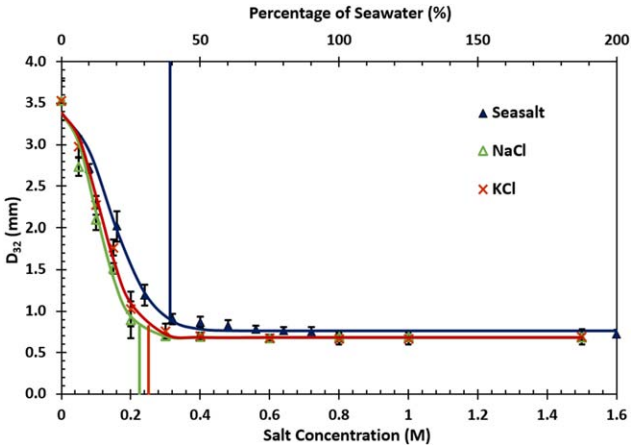

Figure 8. The Sauter mean diameter (D_{32}) as a function of salt concentration for the 1:1 salts and synthetic sea salt, with the altered Nesset model (Eq. 7) and CCC_{95} values indicated. (Error bars represent 95% confidence intervals).

[Color figure can be viewed in the online issue, which is available at wileyonlinelibrary.com.]

trend. The adjusted Nesset model (Eq. 7) was fitted to all the data to determine a critical coalescence ionic strength (CCIS) which was found to be 0.28. The CCIS values for the individual salts are shown in Table 3. The data for the sea salt solution were included in Figure 10 to show the correlation between inorganic salt mixtures and single inorganic salt solutions. Ionic strength of the sea salt was calculated using Eq. 10[27] and the chemical breakdown of the synthetic sea salt as detailed by Atkinson and Bingman[28]

$$I = \frac{1}{2}\sum \frac{m_i}{m^\circ} z_i^2 \tag{10}$$

In this definition of ionic strength, I (dimensionless): z_i is the number of charges on the ion; m_i is the ionic concentration: moles of the ion per kilogram of solution (mol/kg); and m° is

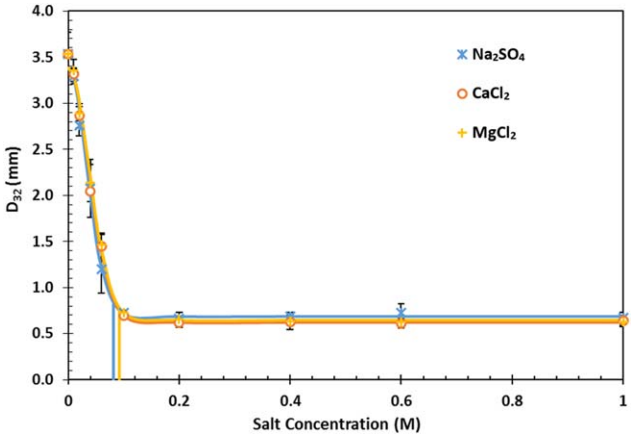

Figure 9. The Sauter mean diameter (D_{32}) as a function of salt concentration for the 2:1 salts, with the altered Nesset model (Eq. 7) and CCC_{95} values indicated. (Error bars represent 95% confidence intervals).

[Color figure can be viewed in the online issue, which is available at wileyonlinelibrary.com.]

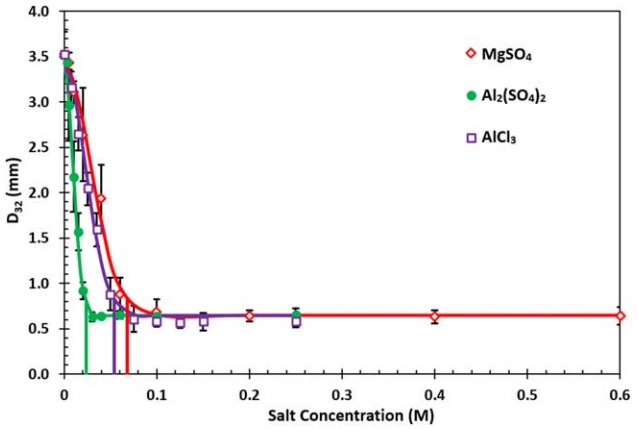

Figure 10. The Sauter mean diameter (D_{32}) as a function of salt concentration for the 2:2, 3:1, and 3:2 salts, with the altered Nesset model (Eq. 7) and CCC_{95} values indicated. (Error bars represent 95% confidence intervals).

[Color figure can be viewed in the online issue, which is available at wileyonlinelibrary.com.]

a standard used to make the ionic strength dimensionless and is equal to 1 mol/kg.[27]

Discussion

In a mechanically agitated vessel, the bubbles cannot be measured *in situ*, as such an accurate representation of the BSD is limited by the bubbles behavior once they have exited the vessel. Issues include hydrostatic pressure (hence volume) changes due to the increase in vertical displacement; probability of coalescence due to the restricted lateral movement and increased manipulation of the bubbles; and even bubble break-up in certain capillary-tube systems. The employment of photography and imaging analysis can introduce further errors, including individual bubble discrimination, resolution, partially captured bubbles, shape identification, or the number of bubbles required for statistically meaningful data.

Visual tracking of bubbles rising in the sampling tube suggested that there was no coalescence or break up caused by the bubbles' restricted motion. As a comparison, Krishna et al.[29] found that a bubble to tube ratio of 0.125 and smaller removed wall effects on the rise velocity of a bubble. The bubble to tube ratio in this experiment for the largest bubble was approximately 0.3, but for the average size it was 0.18. This ratio leads to a maximum reduction in rise velocity of 16% and was, therefore, deemed acceptable for this

Table 3. Critical Coalescence Concentrations (CCC) and Critical Coalescence Ionic Strength (CCIS) for All Salt Types, With the Respective 95% Confidence Intervals (CI)

Salt	CCC	95% CI	CCIS	95% CI
NaCl	0.224	0.008	0.224	0.011
KCl	0.252	0.009	0.252	0.009
$NaSO_4$	0.082	0.003	0.245	0.010
$CaCl_2$	0.091	0.004	0.274	0.012
$MgCl_2$	0.092	0.004	0.277	0.012
$MgSO_4$	0.071	0.003	0.283	0.011
$AlCl_3$	0.056	0.002	0.336	0.012
$Al_2(SO_4)_3$	0.024	0.001	0.354	0.012
Sea salt	0.392	0.017	0.267	0.012

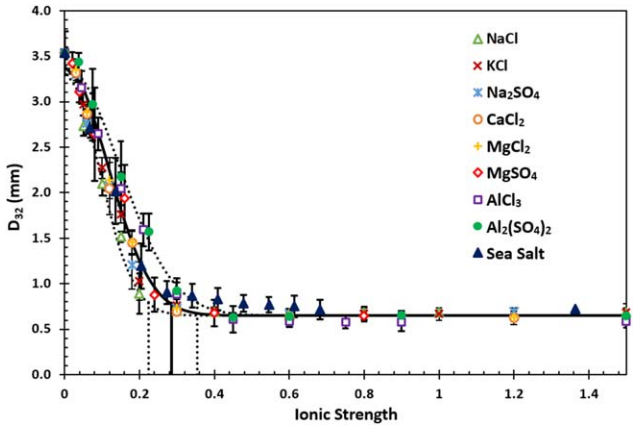

Figure 11. The Sauter mean diameter (D_{32}) as a function of ionic strength for the tested salts and synthetic sea salt, with the averaged altered Nesset model (Eq. 7) and CCIS value indicated. Dashed lines present the range of CCIS curves for all the data. (Error bars represent 95% confidence intervals).

[Color figure can be viewed in the online issue, which is available at wileyonlinelibrary.com.]

application as for coalescence to occur the bubble flow pattern must be altered dramatically. It was assumed that any coalescence events would most likely take place instantly after leaving the turbulent zone and by the time the bubbles reached the sampling tube they had reached a stable final size. Bailey et al.[30] estimated, conservatively, that 1 out of every 1000 bubbles will coalescence inside of the McGill Bubble Viewer system. To test this theory, a larger 30-mm sample tube was used but it was found to not alter the results. The smaller tube was then kept to limit any flow disruption caused by the sample tube in the cell.

Sample location is also of high importance, it has been shown that sampling bubbles close to the wall of the cell (as in this experiment) gives a smaller average bubble size then sampling above the impeller region.[23,31] This is possibly due to large bubbles, with a high buoyancy, not being able to make their way to the side of the cell quick enough to be sampled by the tube. As the geometry of the Denver cell restricts the sampling location to the edges of the cell, bubble size at low concentrations (large bubble size) will be underestimated. Errors associated with bubble sized measurements also increased as solute concentration decreased and was at a maximum for the water tests. This gives further validation to the alterations made to the Nesset model and gives reason to why the original Nesset model overestimated the CCC value.

The validation of the experimental protocol has been detailed by Quinn et al.[9] The commercial frothers DF250 and MIBC were used as they have been well characterized, and this allowed for the comparison of the test results with those from literature. It was found that the results correlated well with literature. Although a larger cell would be preferred in order to allow for conditions closer to those found in industrial applications, the amount of salt needed for repeat tests was deemed unviable: practically and economically.

To the authors' knowledge, there has been no attempt to correlate the TCs of a mixture of inorganic salts with those of single inorganic salts. This was achieved in this study using a synthetic sea salt solution. Instant Ocean© was used as it has been shown to be the closest commercial synthetic mix of seawater salts.[28] It was found that when the multicomponent solution was broken down into its constituent parts, the addition of the ionic strength of each ion correlated well with the overall ionic strength curve of all the salts tested. The CCIS for the sea salt (0.26) lies comfortably within the range of the other salts, 0.22–0.28, excluding the aluminium salts. This variance for salts containing trivalent ions could be attributed to the hydrolysis or their incomplete dissociation.[7] This finding will allow for simpler estimations of bubble size in flotation processes taking place within multicomponent electrolyte solutions.

While other researchers[5,7,9] have presented similar trends with respect to the ionic strength correlation, it is not clear what the underlying mechanism is. Although it is noted that the immobility of the interface by the Marangoni effect is present, with one author stating it is the dominant mechanism,[15] it is theorized that this force is too small to account for the hydrophobic attraction, which is of sufficient magnitude to overcome the hydrodynamic repulsion between two bubbles. In conjunction with the Marangoni effect, electrolytes are said to lower the attractive hydrophobic force between approaching bubbles by hydrating their surfaces.[7,32–34] This is suggested as the main mechanism for the bubble coalescence inhibition. It is also reported that the reduction in the attraction force is a function of ionic strength,[34] further supporting the theory.

Outside the range of salts tested, ionic strength cannot be used confidently as a metric for coalescence inhibition. It has been shown that some inorganic salts show no inhibition qualities (e.g., HCl and H_2SO_4[7]) or that certain 1:1 (cation:anion charge) salts show extremely weak coalescence inhibition (e.g., $NaClO_4$, KI, and KNO_3[4,14]) and as such do not follow the ionic strength rule. The Hofmeister series, which orders salts based on their effect on the solubility of proteins, is typically used for analyzing the ion-specific effects of salts. Although this concept of allows one to understand the general effect of salts on bubble coalescence, it does not align with the observations concerning the inhibiting effect of all salts on bubble coalescence.[13] Based on information from molecular dynamic simulations and sum frequency generation spectroscopy, the ion-specific effects have instead been theorized to be caused by the tendencies of the ions to be attracted or repelled from the air-water interface. Salts which have, from their cation/anion pair, one ion with an affinity for the interface and the other for the bulk will inhibit bubble coalescence.[13] This explained the originally empirical formulation of the cation/anion pair rules developed by Craig et al.[7]

Another discrepancy from the ionic strength correlation is the degree to which atoms within the same periodic group

Table 4. Comparison of Transition Concentrations and CCC_{95} Values Found in Literature for Group 1 and 2 Chlorides

Author	KCl	NaCl	LiCl	$CaCl_2$	$MgCl_2$
Lessard and Zieminski (1971)[5]	0.23	0.175	0.16	0.055	0.055
This work	0.25	0.22		0.09	0.09
Zahradnik et al. (1999)[11]	0.202	0.145			
Craig et al. (1993)[7]	0.12	0.078			
Quinn et al. (2014)[9]	0.31	0.31			
Firouzi, Howes, and Nguyen (In press)[13]	0.15	0.1			

inhibit coalescence. If a comparison is made with the cations within the alkali group, when attached to chloride atoms, a distinct trend is seen (Table 4). With the exception of Quinn et al.[9] (whose CCC_{95} results had a 95% confidence interval of 0.8 M) all TCs reported in literature show a reduction in magnitude from KCl to NaCl, with a further reduction for LiCl (only tested in one study). This further supports that ion-specificity is important in determining coalescence inhibition. However, if the alkaline earth metals are compared there is no difference in TC for $MgCl_2$ and $CaCl_2$ from this work and the work of Lessard and Zieminski.[5] Although this could be due to the precision of the measurements.

Conclusions

The CCC was determined for a series of coalescence inhibiting inorganic salts (NaCl, KCl, Na_2SO_4, $CaCl_2$, $MgCl_2$, $MgSO_4$, $AlCl_3$, and $Al_2(SO_4)_3$) and a synthetic a sea salt solution. The CCC values ranged from 0.02 M ($Al_2(SO_4)_3$) to 0.25 M (KCl), with the CCC decreasing for salts containing multivalent ions. The decrease in bubble size correlated with ionic strength giving a CCIS of 0.28. It was found that when the multicomponent sea salt solution was broken down into its constituent parts, the addition of the ionic strength of each ion correlated well with the overall ionic strength curve of all the salts tested.

Acknowledgment

The authors would like to acknowledge the Natural Sciences and Engineering Research Council of Canada (NSERC) and Vale Base Metals, Teck Resources Ltd., Xstrata Process Support, Barrick Gold Corp., Shell Canada Ltd., SGS Canada Inc., COREM, and CheMIQA for funding this work through the Collaborative Research and Development (CRD) program (CRDPJ 445682-12).

Literature Cited

1. Cho YS, Laskowski JS. Bubble coalescence and its effect on bubble size and foam stability. *Can J Chem Eng*. 2002;80:299–305.
2. Grau RA, Laskowski JS, Heiskanen K. Effect of frothers on bubble size. *Int J Miner Process*. 2005;76:225–233.
3. Foulk CW, Miller JN. Experimental evidence in support of the balanced layer theory of liquid film formation. *J Ind Eng Chem*. 1931; 23(11):1283–1288.
4. Marrucci G, Nicodemo L. Coalescence of gas bubbles in aqueous solutions of inorganic electrolytes. *Chem Eng Sci*. 1967;22:1257–1265.
5. Lessard RD, Zieminski SA. Bubble coalescence and gas transfer in aqueous electrolytic solutions. *Ind Eng Chem Fundam*. 1971;10:260–289.
6. Quinn JJ, Kracht W, Gomez CO, Gagnon C, Finch JA. Comparing the effects of salts and frother (MIBC) on gas dispersion and froth properties. *Miner Eng*. 2007;20:1296–1302.
7. Craig VSJ, Ninham BW, Pashley RM. The effect of electrolytes on bubble coalescence in water. *J Phys Chem*. 1993;97:10192–10197.
8. Kim JW, Chang JH, Lee WK. Inhibition of bubble coalescence by the electrolytes. *Korean J Chem Eng*. 1990;7(2):100–108.
9. Quinn JJ, Sovechles JM, Finch JA, Waters KE. Critical coalescence concentration of inorganic salt solutions. *Miner Eng*. 2014;58:1–6.
10. Cho YS, Laskowski JS. Effect of flotation frothers on bubble size and foam stability. *Int J Miner Process*. 2002;64:69–80.
11. Zahradnik J, Fialová M, Linek V. The effect of surface additives on bubble coalescence in aqueous media. *Chem Eng Sci*. 1999;54:4757–4766.
12. Wang B, Peng Y. The effect of saline water on mineral flotation – a critical review. *Miner Eng*. 2014;66–68:13–24.
13. Firouzi M, Howes T, Nguyen AV. A quantitative review of the transition salt concentration for inhibiting bubble coalescence. *Adv Colloid Interface Sci*. In Press. DOI: 10.1016/j.cis.2014.07.005.
14. Christenson HK, Bowen RE, Carlton JA, Denne JRM, Lu Y. Electrolytes that show a transition to bubble coalescence inhibition at high concentrations. *J Phys Chem C*. 2008;112:794–796.
15. Prince MJ, Blanch HW. Transition electrolyte concentrations for bubble coalescence. *AIChE J*. 1990;36(9):1425–1429.
16. Zieminski SA, Whittemore RC. Behavior of gas bubbles in aqueous electrolyte solutions. *Chem Eng Sci*. 1971;26:509–520.
17. Keitel G, Onken U. Inhibition of bubble coalescence by solutes in air/water dispersions. *Chem Eng Sci*. 1982;37(11):1635–1638.
18. Alexander S, Quinn JJ, Finch JA. Correlation of graphite flotation and gas holdup in saline solutions. In: *Water in Mineral Processing: Proceedings of the First International Symposium*. Englewood, CO: SME, 2012.
19. Castro S, Toledo P, Laskowski JS. Foaming properties of flotation frothers at high electrolyte concentration. In: *Water in Mineral Processing: Proceedings of the First International Symposium*. Englewood, CO: SME, 2012.
20. Gomez CO, Finch JA. Gas dispersion measurements in flotation machines. *CIM Bull*. 2002;95(1066):73–78.
21. Hernandez-Aguilar JR, Coleman RG, Gomez CO, Finch JA. A comparison between capillary and imaging techniques for sizing bubbles in flotation systems. *Miner Eng*. 2004;17(1):53–61.
22. Gomez CO, Finch JA. Gas dispersion measurements in flotation cells. *Int J Miner Process*. 2007;84(1–4):51–58.
23. Hernandez-Aguilar JR, Gomez CO, Finch JA. A technique for the direct measurement of bubble size distributions in industrial flotation cells. In: 34th Annual Meeting of the Canadian Mineral Processors. Ottawa, Canada: CIM, 2002.
24. Quinn JJ, Maldonando M, Gomez CO, Finch JA. Experimental study on the shape–velocity relationship of an ellipsoidal bubble in inorganic salt solutions. *Miner Eng*. 2014;55:5–10.
25. Nesset JE, Finch JA, Gomez CO. Operating variables affecting the bubble size in forced-air mechanical flotation machines. In: Proceedings of the 9th Mill Operators Conference. AusIMM, Fremantle, Australia, 2007.
26. Gomez CO, Alvarez J, Castillo P. A frother characterisation technique using a lab mechanical flotation cell. In: XXVII International Mineral Processing Congress. Gecamin, Santiago, Chile, 2014.
27. Solomon T. The definition and unit of ionic strength. *J Chem Educ*. 2001;78(12):1691–1692.
28. Atkinson MJ, Bingman C. Elemental composition of commercial seasalts. *J Aquariculture Aquat Sci*. 1998;8(2):39–43.
29. Krishna R, Urseanu MI, van Baten JM, Ellenberger J. Wall effects on the rise of single gas bubbles in liquids. *Int Commun Heat Mass Transf*. 1999;26(6):781–790.
30. Bailey M, Torrealba-Vargas J, Gomez CO, Finch JA. Coalescence of bubbles sampled for imaging. *Miner Eng*. 2005;18(1):125–126.
31. Gorain BK, Franzidis JP, Manlapig EV. Studies on impeller type, impeller speed and air flow rate in an industrial scale flotation cell - part 1: effect of bubble size distribution. *Miner Eng*. 1995;8(6):615–635.
32. Tsang YH, Koh Y-H, Koch DL. Bubble-size dependence of the critical electrolyte concentration for inhibition of coalescence. *J Colloid Interface Sci*. 2004;275:290–297.
33. Chan BS, Tsang YH. A theory on bubble-size dependence of the critical electrolyte concentration for inhibition of coalescence. *J Colloid Interface Sci*. 2005;286:410–413.
34. Manciu M, Ruckenstein E. Role of the hydration force in the stability of colloids at high ionic strengths. *Langmuir*. 2001;17(22):7061–7070.

Manuscript received Nov. 28, 2014, and revision received Apr. 7, 2015.